

Electron acceleration behind a wavy dipolarization front

Mingyu Wu¹ · Quanming Lu²  · Martin Volwerk³ · Rumi Nakamura³ · Tielong Zhang^{1,3}

Received: 9 October 2017 / Accepted: 21 December 2017
© Springer Science+Business Media B.V., part of Springer Nature 2018

Abstract In this paper, with the in-situ observations from the Time History of Events and Macroscale Interactions during Substorms (THEMIS) probes we report a wavy dipolarization front (DF) event, where the DF has different magnetic structures and electron distributions at different y positions in the Geocentric Solar Magnetospheric (GSM) coordinates. At $y \sim 2.1R_E$ (R_E is the radius of Earth), the DF has a relatively simple structure, which is similar to that of a conventional DF. At $y \sim 3.0R_E$, the DF is revealed to have a multiple DF structure, where the plasma exhibits a vortex flow. Such a wavy DF could be the results of the interchange instability. The different structure of such a wavy DF at different sites has a great effect on electron acceleration. Fermi acceleration can occur at the site of the DF with a simple or multiple DF structure, while betatron acceleration as a local process has the contribution to energetic electrons only at the site of the DF with a simple structure.

Keywords Dipolarization front · Electron acceleration · Betatron acceleration

1 Introduction

Dipolarization fronts (DFs), the transient enhancements of the northward component of magnetic field, are always observed at the leading edge of bursty bulk flows (BBFs) in

the magnetotail (Nakamura et al. 2002b; Runov et al. 2009; Ohtani et al. 2004). As a boundary with a typical scale of about 1–2 ion inertial lengths, DFs are tangential discontinuities (Schmid et al. 2011), which can separate BBFs from the ambient plasma sheet (Ohtani et al. 2004). There is also a possibility that DFs are the earthward propagating flux rope (Vogiatzis et al. 2015; Lu et al. 2015b). DFs can be formed during jet braking (Birn et al. 2011), by spontaneous formation (Sitnov et al. 2013) or transient reconnection (Sitnov et al. 2009; Fu et al. 2013), and they are found to play an important role in accelerating electrons through betatron and Fermi mechanisms (Fu et al. 2011; Pan et al. 2012; Wu et al. 2013, 2015; Runov et al. 2013; Lu et al. 2016). Betatron acceleration caused by the compression of magnetic field at DFs leads to the enhancement of energetic electron flux at the pitch angle around 90° (Ashour-Abdalla et al. 2011; Fu et al. 2011; Pan et al. 2012; Wu et al. 2013; Wang et al. 2016), while Fermi acceleration due to the contraction of mirror distance causes the enhancement of energetic electron flux at pitch angles around 0° and 180° (Birn et al. 2014; Fu et al. 2011; Pan et al. 2012; Wu et al. 2013; Wang et al. 2016). The energetic electrons generated during DFs are suggested to be related to aurorae and substorms (Volwerk et al. 2008; Ashour-Abdalla et al. 2011).

However, as DFs propagate earthward from the mid-tail to the near-Earth region, the interchange/ballooning instability may self-consistently develop (e.g. Lu et al. 2013, 2015a; Lapenta and Bettarini 2011) and changes the magnetic field configuration of DFs. Then, the DFs evolve into a wavy shape along the dawn-dusk direction (Nakamura et al. 2002a). Using an ideal magnetohydrodynamics (MHD) model, Guzdar et al. (2010) found that DFs can develop into mushroom-like structures during the excitation of the interchange instability. Moreover, three-dimensional

✉ Q. Lu
qmlu@ustc.edu.cn

¹ Harbin Institute of Technology, Shenzhen, China
² CAS Key Laboratory of Geospace Environment, Department of Geophysics and Planetary Science, University of Science and Technology of China, Hefei, China
³ Space Research Institute, Austrian Academy of Science, Graz, Austria

(3D) particle-in-cell (PIC) simulations have revealed that the wavelength of the structures of DFs along the dawn-dusk direction caused by the kinetic interchange instability can be down to about several ion Larmor radii (Pritchett and Coroniti 2010, 2011; Vapirev et al. 2013; Pritchett 2015). These numerical studies indicated that the DF has a complex three-dimensional (3D) structure and cannot be simply taken as a large R_E -size smooth interface along the dawn-dusk direction. Until now, how the structure developed due to the interchange instability in DFs will influence electron acceleration has never been investigated. In this paper, for the first time, we simultaneously observe a DF at different sites along the dawn-dusk direction with two spacecraft of the THEMIS probes, and find that the DF has different structures at different sites. Such structures could be attributed to the results of the interchange instability, and electron accelerations are then investigated at such a wavy DF.

In our work, we use the magnetic field data from the fluxgate magnetometers (FGM) (Auster et al. 2008), low energy (5 eV–30 keV) particle data from the electrostatic analyzer

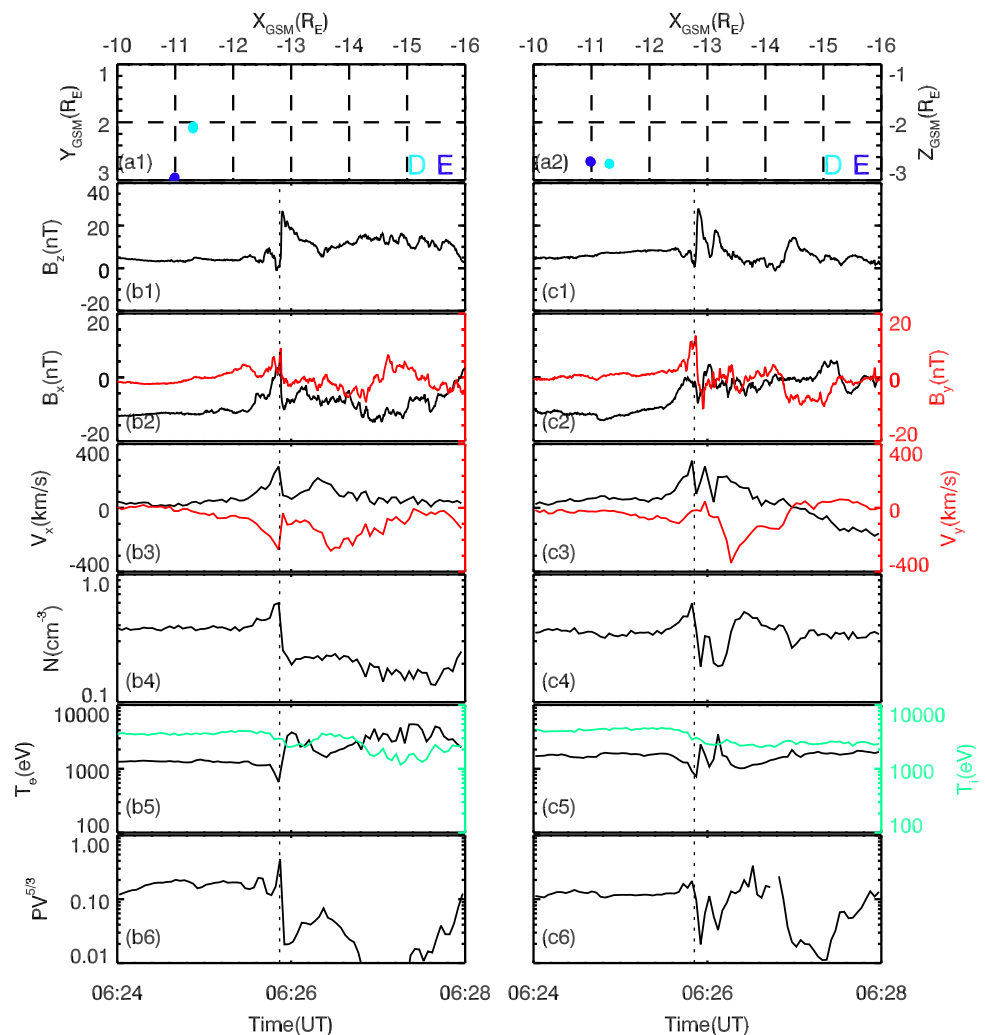
(ESA) (McFadden et al. 2008) and high energy (30 keV–1 MeV) particle data from the Solid State Telescope (SST) (Angelopoulos 2008). FGM provides 4 Hz resolution DC magnetic field data. Additionally, it can also provide DC magnetic field data with 128 Hz sample rates in the burst mode. ESA and SST can provide ion and electron distribution functions with a time resolution of 3 s. All the data used in this paper are in the GSM coordinates unless noted otherwise.

2 Observation results

Based on a dual observation of THEMIS in the near-Earth tail on 22 February 2008, we report a wavy DF event seen by THD and THE, and emphatically analyze the electron distributions behind this wavy DF.

Figure 1 gives the overview of this DF event. The first panel of Fig. 1 shows the locations of THD (cyan point) and THE (blue point) in GSM (a1) x - y and (a2) x - z

Fig. 1 The overview of the DF event on 22 February 2008. The top panel shows positions of two spacecraft THD and THE in (a1) x - y and (a2) x - z planes. From the second to the last panels of the figure, the left column shows (b1) the z component of magnetic field B_z , (b2) B_x (black line) and B_y (red line), (b3) plasma bulk velocity v_x (black line) and v_y (red line), (b4) plasma density N , (b5) electron temperature T_e (black line) and ion temperature T_i (green line), and (b6) the local flux tube entropy $PV^{5/3}$ observed by THD. The right columns (c1)–(c6) with the same format as the left column, shows the magnetic field and particle observation results of THE. The vertical dashed black lines show the arrival time of the DF



planes. During the time interval 06:24–06:32 UT, THD located near $[-11.3, 2.1, -2.7]R_E$, while THE is near $[-11.0, 3.0, -2.7]R_E$. These two spacecraft are both located in what is usually assumed to be the braking region. The separation between THD and THE is mainly along the y direction, while the separation along x or z direction of the two spacecraft is very short.

From the second to the last panels of Fig. 1, the left and right columns show the magnetic field B_z , B_x (black line) and B_y (red line), the bulk velocity v_x (black line) and v_y (red line), plasma density N , electron temperature T_e (black line) and ion temperature T_i (green line), and the local flux tube entropy $PV^{5/3}$ of THD and THE, respectively. In Fig. 1, the magnetic field data has a time resolution of 0.25 s while the others have a time resolution of 3 s. Initially, THD detects a steady plasma sheet with $B_z \sim 5$ nT. THE is also in a steady plasma sheet. But because THE is closer to the Earth than THD, the B_z of the plasma sheet is about 8 nT which is a bit higher than the observation results of THD. At about 06:25:52 UT, a front-like variation in B_z from 0 nT to 27 nT was detected by THD and characterized as a DF. Ahead of the DF it is a dip of B_z which lasts about 4 s. Like THD, a DF, characterized by a sharp jump of B_z from 0 nT to 28 nT, is detected by THE at about 06:25:51 UT. Ahead of this DF it is also a dip of B_z . THD and THE have almost simultaneously observed a DF event. Previous studies have confirmed that DFs can expand $1 \sim 3R_E$ in the dawn-dusk direction (Liu et al. 2015; Huang et al. 2015b), so the DF observed by THD and THE which are only separated about $0.9R_E$ along the y direction can be the same one observed by two spacecraft at different locations in the near-Earth tail. In Fig. 1, the arrival time of this two-points observed DF is marked by the vertical dashed lines.

Before the arrival of the DF, both two spacecraft observed a high speed flow with $v_x \sim 300$ km/s and a negative v_y . This high speed flow has a high plasma density and a low electron temperature. This flow is the precursor flow and its features fit previous observation and simulation results well (Zhou et al. 2010). After crossing the DF, two spacecraft enter into a BBF region. The peak value of v_x of this BBF observed by THD is about 190 km/s, and v_x observed by THE can reach about 240 km/s. The difference of peak values of v_x suggest a possibility that THE is closer to the center of flow channel than THD. In the BBF of this event, plasma density is about 0.2 cm^{-3} and the magnitude of magnetic field is about 30 nT. So the Alfvén velocity is about 1500 km/s. The observed BBF is an indeed subsonic flow. The small flow velocity could be due to the flow breaking process. An interesting thing is that THE observed the simultaneous reversal of v_x and v_y behind the DF. In the braking region, the flow reversal could be caused by the rebound of a BBF (Panov et al. 2010).

Furthermore, in this event THE observed two B_z jumps which are around 06:25:51 UT and 06:26:02 UT, respectively. Such two B_z jumps are always considered to be multiple DFs (Zhou et al. 2009; Hwang et al. 2011). We can name the first B_z jump as DF1, and the second B_z jump as DF2. During the time interval 06:25:51–06:26:25 UT, the two jumps are evident in B_z , plasma density N , and electron temperature T_e . The v_x displays a unipolar structure with a maximum value ~ 240 km/s, while the v_y displays a dipolar structure with the value from ~ 40 km/s to ~ -350 km/s. Besides, v_x has a maximum value between DF1 and DF2. Using MHD simulations Guzdar et al. (2010) have demonstrated that multiple DFs caused by the interchange instability can have these features: multiple jumps of B_z and plasma density, unipolar v_x , and bipolar v_y . In their simulations, the subsonic flow associated with the DF has its maximum v_x between two DFs. Our observation results are consistent with the prediction of MHD simulations. All these features suggest a possibility that because of the interchange instability the observed DF in our event evolves into a mushroom-like structure and have a wavy shape. Then THE passes this wavy DF, and has detected DF1 and DF2.

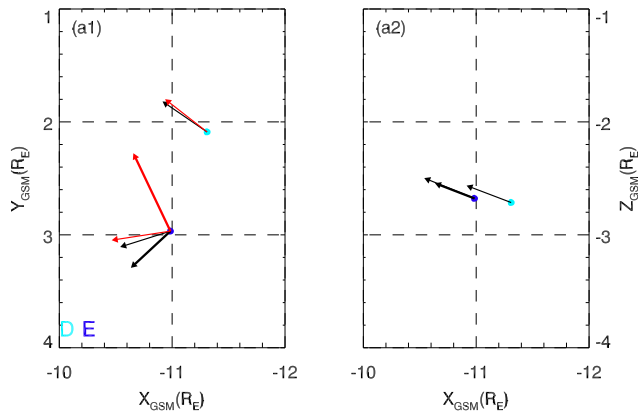
The formation of mushroom-like structures of dipolarization fronts showed by Guzdar et al. (2010) require a long time. In this event, the probes THB and THC are located at about $-24R_E$ and $-18R_E$, respectively. Both THB and THC have detected earthward flows (not shown). It suggests that the BBF observed by THD and THE originates from the region further than $-24R_E$. So the observed DF as the leading edge of the BBF, can at least propagate about $13R_E$. The velocity of the BBF in the magnetotail is less than the local Alfvén velocity which is normally about 1000 km/s (Angelopoulos et al. 1992). The evolution time of the DF should be more than $13R_E/V_A$. There is enough time to form such structures for our event.

In Fig. 1(b5) and (c5), we can find that as this wavy DF passes by, the electron temperature has a sharp increase. The electron temperature T_e behind the DF is about 3 keV, which is about 2 times higher than that in the upstream plasma sheet. Besides, in Fig. 1(c5) the peak value of T_e behind DF1 is a bit smaller than the peak value of T_e behind DF2. In the upstream plasma sheet, the ion temperature T_i is about 4 keV, which is about 3 times higher than the electron temperature T_e . However, after crossing the DF T_i has a decrease. In Fig. 1(b5), behind the DF the electron temperature T_e is higher than T_i . In Fig. 1(c5), behind DF1 T_e is a little smaller than T_i while behind DF2 T_e is higher than T_i .

We use the method in Wolf et al. (2006) to calculate the entropy $PV^{5/3}$ of the flux tube. Their method assumes an inverse entropy dependence on the z component of the magnetic field B_z . In Fig. 1(b6) and (c6), the flux tube entropy has a sharp decrease at each crossing of the DF. Additionally, the flux tube entropy increase in the tailward flow ob-

Table 1 Normal direction of the dipolarization front obtained from MVA of the Magnetic Field detected by THD and THE

SC	Time interval	n_x	n_y	n_z	λ_2/λ_3
THD	06:25:49–06:25:56	0.79	−0.54	0.30	16.7
THE	06:25:45–06:25:59	0.89	0.28	0.36	11.5
THE	06:26:01–06:26:11	0.70	0.66	0.27	11.2

**Fig. 2** The normal direction of the DF projected in the (a1) x - y and (a2) x - z planes. The flow directions are also plotted by red arrows. At the location of THE, the thin black and red arrows represent the results of DF1, while the thick black and red arrows represent the results of DF2

served by THE. Such a tailward flow is a natural consequence of interchange-unstable flux tube propagating earthwards, which has also been reported in previous work (e.g. Walsh et al. 2009; Panov et al. 2010).

With single-point magnetic field measurements, the normal direction $\mathbf{n} = (n_x, n_y, n_z)$ of this wavy DF can be estimated by minimum variance analysis (MVA) method. The normal direction \mathbf{n} and the eigenvalue ratio λ_2/λ_3 between the minimum and medium variance direction are listed in Table 1. The large eigenvalue ratio indicates the good quality of the method to calculate the normal direction. Figure 2 shows the normal direction (black arrows) for the THD and THE projected in the (a1) x - y and (a2) x - z planes. The flow velocities are also plotted with red arrows. For THE, the thin black and red arrows represent the results of DF1, while the thick black and red arrows represent the results of DF2. In Fig. 2(a1), the opposite sign of n_y indicates that THD and THE are located at the two different flanks of this wavy DF. THD at $y \sim 2.1R_E$ is located at the dawnside flank of this wavy DF while THE at $y \sim 3.0R_E$ is located at the duskside flank of this wavy DF. At the dawnside flank, THD observed a flow velocity which is nearly parallel to the normal direction of the DF. At the duskside of this wavy DF, we can find that there is an obvious angle between the normal directions of DF1 and DF2 observed by THE, the flow velocity also changes its direction. The flow velocity behind

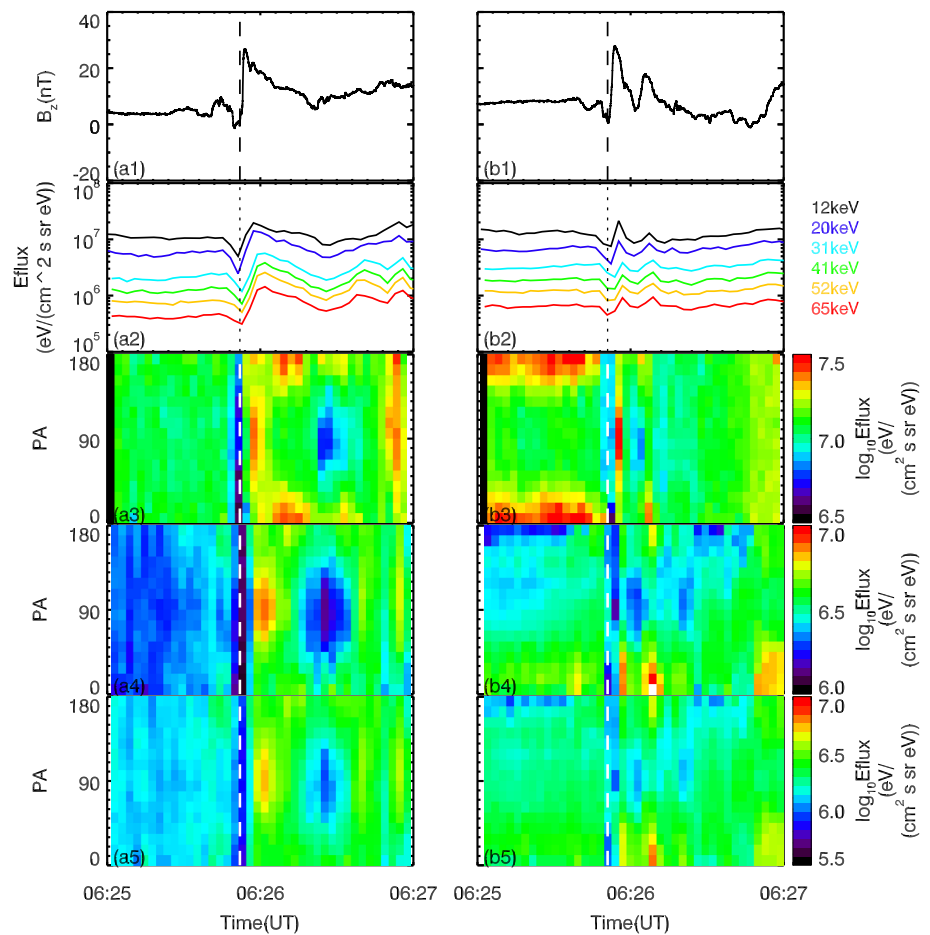
DF2 is nearly perpendicular to the normal direction of DF2. The observed normal directions of the DF at different site also indicate that the DF has a wavy shape in the x - y plane. In Fig. 2(a2), the similar n_x and n_z suggest that THD and THE have crossed the similar position of this wavy DF in the x - z plane.

Figure 3 shows the z component of the magnetic field B_z with 128 Hz data, the differential energy fluxes of energetic electrons, and the electron energy flux pitch angle distributions versus time for different energy ranges observed by the THEMIS ESA and SST instruments for (left) THD and (right) THE, respectively. The particle data is obtained in the burst mode and has a time resolution of 3 s. In the Fig. 3(a2) and (b2), the lowest two energy channels were measured by ESA, and other channels in the energy range from 31 keV to 65 keV were measured by SST instrument. We can find that energetic electron energy flux in all energy channels just behind the DF has a sharp increase and the value of energy flux quickly reaches its maximum. Furthermore, in Fig. 3(b2) we can find that the peak values of energetic electron energy flux with energy 12 keV behind DF1 are higher than that behind DF2, but the peak values with the energies range from 20 keV to 65 keV behind DF1 and DF2 are similar.

From the third to the bottom panel, the pitch angle distributions are for the energy 12 keV, 31 keV, 42 keV, and the scale on the y axis gives electron pitch angles with 0° (parallel) at the bottom and 180° (anti-parallel) at the top of each panel. As shown in Fig. 3(a3)–(a5), the perpendicular distribution behind the DF in all three energy channels are observed by THD. In Fig. 3(a3) and (a4), we can also find that there is an enhancement of electron energy flux within energies 12 keV and 31 keV at the pitch angle around 180° . As shown in Fig. 3(b3)–(b5), the electron distributions observed by THE are a bit complex. Behind the DF1, electrons with energy 12 keV have a perpendicular distribution, while electrons with energies 31 keV and 42 keV have a field-aligned distribution. Behind the DF2, energetic electrons have a field-aligned distribution in all three energy channels.

Figure 4 shows the detailed pitch angle distributions from THD and THE behind the DF for 15 different energy channels from 0.3 keV to 140 keV with 3 s resolution. The pitch angle distributions in solid curves are obtained from the measurements of ESA, and the others in dashed curves are obtained from the measurements of SST. Figure 4(a) shows the electron phase space density distribution at the time when the energetic electron energy flux behind the wavy DF observed by THD reaches the first peak value. In Fig. 4(a), electrons with lower energies range from 0.3 keV to 5 keV have field-aligned distributions while energetic electrons with higher energies range from 15 keV to 100 keV have perpendicular distributions. But electrons in the energy channel 139 keV have an isotropic distribution. Figure 4(b) shows the electron phase space density distribution

Fig. 3 The left column is the observation results of THD, while the right column is the results of THE. The top panel contains the three components of the magnetic field with 128 Hz data. The second panel shows the differential energy fluxes of energetic electrons. The next three panels contain electron pitch angle distributions in the energy channel 12 keV, 31 keV and 42 keV, respectively. The vertical dashed lines show the arrival time of the DF



at the time when the energetic electron energy flux behind the DF1 reaches the first peak value. In Fig. 4(b), electrons with lower energies range from 0.3 keV to 5 keV have field-aligned distributions, and energetic electrons with higher energies range from 20 keV to 140 keV also have field-aligned distributions. But electrons with energies range from 8.8 to 15 keV have perpendicular distributions. Figure 4(c) shows the electron phase space density distribution at the time when the energetic electron energy flux behind the DF2 reaches the first peak value. In Fig. 4(c), energetic electrons with energies range from 8.8 keV to 140 keV have field-aligned distributions. Besides, in Fig. 4(b) and (c) we note that phase space densities of energetic electrons with energies range from 20 keV to 140 keV at the pitch angle around 0° is higher than that around 180°. Furthermore, phase space densities of energetic electrons with energies from 20 keV to 100 keV at the pitch angle around 90° in Fig. 4(a) are about 2–4 times higher than that in Fig. 4(b) and (c).

3 Discussion

In this paper, we have studied the electron acceleration process behind a wavy DF. Figure 5 gives the sketch of this

wavy DF event in the x – y plane. The gray boundary gives a possible configuration of the wavy DF. The dashed black arrows show the possible trajectories of spacecraft, and the solid red arrows show the local flow velocities.

The upper part of the DF has a relatively simple and steady structure. THD passes the DF along the upper dashed black arrow, and has observed a conventional DF. The BBF's velocity is nearly parallel to the normal direction of the DF. In such case the BBF can continuously compress the magnetic field and then lead to the betatron acceleration which cause the enhancement of phase space densities of energetic electrons at the pitch angle around 90°. Previous two-dimensional (2-D) particle-in-cell simulations have demonstrated that a parallel electric field exists just behind the DF (Huang et al. 2015a). This parallel electric field can trap energetic electrons with small parallel velocity for a long time. Meantime, the inductive electric field due to the increase of B_z of the DF can accelerate these electrons in the perpendicular direction. Therefore, low energy electrons have a large parallel velocity and form a field-aligned distribution, while energetic electrons which can be energized by betatron acceleration form a perpendicular distribution. As shown in the Fig. 4(a), we can find that low energy electrons with energy

Fig. 4 Electron phase space density distributions (a) behind the wavy DF observed by THD at the time 06:26:00 UT, (b) behind the DF1 observed by THE at 06:25:55 UT, and (c) behind the DF2 observed by THE at 06:26:07 UT

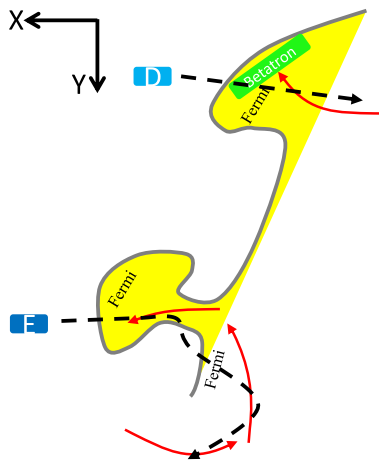
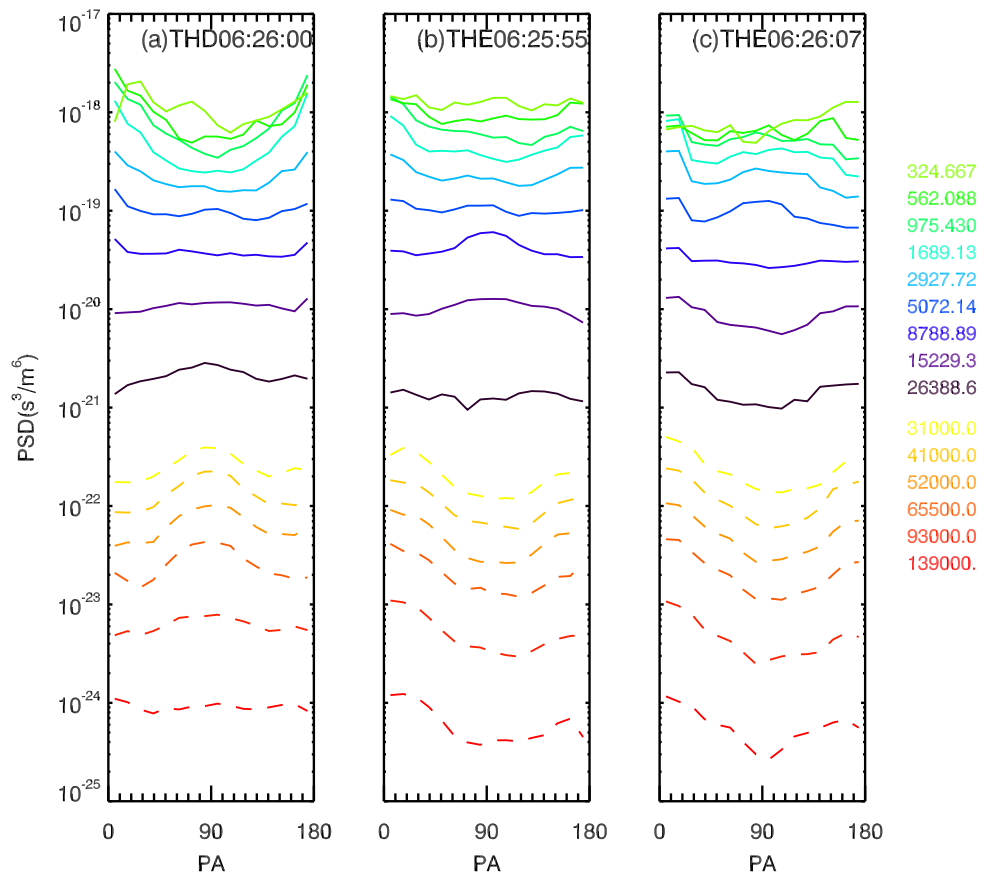


Fig. 5 The sketch of this wavy DF event in the x - y plane. The gray boundary gives the possible configuration of the DF. The dashed black arrows show the possible trajectories of spacecraft. The red arrows show the local flow velocities. The yellow region shows the possible region where Fermi acceleration can occur, while the green region shows the possible region where Betatron acceleration can occur

about several hundred eV have a field-aligned distribution while energetic electrons with energies range from 15 keV to 100 keV have a perpendicular distribution. Our observations fit the theoretical prediction results well. Besides, dur-

ing the earthward propagation of this DF, the shortened mirror distance of energetic electrons can lead to Fermi acceleration which can cause the increase of phase space densities of energetic electrons at pitch angles around 0° and 180° . As shown in Fig. 4(a), it can be found that there is also a small peak around 180° in the energy channel 26 keV and 31 keV. However, betatron acceleration could be very effective for electrons with energy about several tens of keV. For these electrons, though Fermi acceleration also occur at $y \sim 2.1R_E$, this more effective betatron acceleration makes that energetic electron flux at the pitch angle around 90° is higher than that at pitch angles around 0° and 180° . It leads to the observed perpendicular distribution at $y \sim 2.1R_E$.

The under part of the DF has a wavy shape. The multiple jumps of B_z and plasma density, unipolar v_x , and bipolar v_y suggest that the wavy shape could be formed by the interchange instability. In the magnetotail, the flux tube entropy generally increases with increasing distance from Earth. As shown in Fig. 1, the flux tube with the enhanced B_z behind a DF has lower entropy than the upstream plasma sheet. It leads to a gradient of flux tube entropy pointing radially inward when then can cause the interchange instability (Xing and Wolf 2007; Hwang et al. 2011). THE passes the wavy DF and has observed multiple DFs structures. Behind the wavy DF, there is a flow vortex which could be caused by

the flow rebound in the braking region (Panov et al. 2010), which is also a natural result of interchange-unstable flux tube. The complex magnetic structures of the DF and the related flow vortex can affect the electron acceleration process. In the under part, energetic electrons with energies range from 20 keV to 140 keV behind the DF have the field-aligned distribution which could be caused by Fermi acceleration. But the distributions of energetic electrons with energies range from 8.8 keV to 15 keV are different at the different locations. These energetic electrons have a perpendicular distribution behind DF1 when the BBF's velocity is nearly parallel to the normal direction of the DF, while they have a field-aligned distribution behind DF2 when the BBF's velocity is nearly perpendicular to the normal direction of the DF.

Runov et al. (2013) have analyzed several multi-points observed DF events and point out that energetic electrons with energies about tens of keV have the perpendicular distribution near the neutral sheet and field-aligned distribution far away from the neutral sheet. In our event, two spacecraft located in the same position in the z axis. Additionally, the value of B_x is also similar when the two spacecraft observed different electron distributions. So the different electron distributions are not due to the difference of locations in the z direction.

In our event, the local structures of the DF and electron distributions are different along the y direction. Fermi acceleration can occur at the site of the DF with a simple or multiple DF structure, while betatron acceleration as a local process has the contribution to energetic electrons with energies tens of keV only at the limited region of the DF.

4 Conclusions

In this paper, with the observations of THEMIS probes we have studied a wavy DF event. At $y \sim 2.1R_E$ the DF is observed to have a relatively simple and steady structure, which is located at the leading part of a BBF. At $y \sim 3.0R_E$ the DF is observed to have multiple DFs structures, where the plasma exhibits a vortex flow. The multiple DFs structures could be caused by the interchange instability. By crossing the DF, an increase of energetic electron fluxes in the energy range from 12–65 keV is observed. This increase is considered to be caused by adiabatic acceleration mechanisms. Electron distributions behind this wavy DF suggest that the different structure of such a wavy DF at different locations has a great effect on electron acceleration. At $y \sim 3.0R_E$, field-aligned distributions of energetic electrons with energies from 20 keV to 140 keV behind the wavy DF indicate that energetic electrons suffer Fermi acceleration. Fermi acceleration causes energetic electrons with energy about tens of keV just behind the DF have a much

higher energy flux than that in front of the DF. Energetic electrons at the pitch angle around 0° are observed to be higher than that around 180° , which could be related to the complex magnetic field configuration of this wavy DF. But the distributions of energetic electrons with energies range from 8.8 keV to 15 keV behind DF1 and DF2 are different. These energetic electrons have a perpendicular distribution behind DF1 when the BBF's velocity is nearly parallel to the normal direction of the DF, while they have a field-aligned distribution behind DF2 when the BBF's velocity is nearly perpendicular to the normal direction of the DF. At $y \sim 2.1R_E$, behind the relatively simple structure of the DF, the perpendicular distribution of energetic electrons with energies from 15 keV to 100 keV indicates that these electrons suffer betatron acceleration. The isotropic distribution of energetic electrons with energy 139 keV suggests that the upper limit for the acceleration is about 100 keV. During the earthward propagation, the contraction of mirror distance can lead to Fermi acceleration. The enhancement of energy flux of energetic electrons in the energy channels 26 keV and 31 keV at the pitch angle around 180° indicates that Fermi acceleration also occurs. These observation results suggest that Fermi acceleration can occur at the site of the DF with a simple or multiple DF structure, while betatron acceleration as a local process has the contribution to energetic electrons only at the site of the DF with a simple structure. Though DFs are considered to expand about $1\text{--}3R_E$ along the dawn-dusk direction (Liu et al. 2015; Huang et al. 2015b), the region where betatron acceleration works could be very small.

In the near-Earth tail, both the large-scale MHD properties and the small-scale effect of the plasma interaction with the terrestrial dipole field need to be taken into account in the study of electron accelerations (Nakamura et al. 2013). The wavy DF formed by interchange instabilities has complex 3D structures. The local magnetic field configuration and flow features of the DF could have a significant effect on electron energization process. Our study suggests that during the study of electron accelerations, DFs cannot be simply taken as a large R_E -size 2D interface, and the effect of 3D structures of DFs should be included in the modeling of electron energization in the magnetotail.

Acknowledgements This research was supported by the National Science Foundation of China, Grant Nos. 41404129, 41331067, 41527804, 41474125, 41421063, 973 Program (2013CBA01503, 2012CB825602). We acknowledge NASA contract NAS5-02099 and V. Angelopoulos for use of data from the THEMIS Mission, specifically; C.W. Carlson and J.P. McFadden for the use of ESA data; K.H. Glassmeier, U. Auster and W. Baumjohann for the use of FGM data provided under the lead of the Technical University of Braunschweig and with financial support through the German Ministry for Economy and Technology and the German Center for Aviation and Space (DLR) under contract 50 OC 0302. All the data of THEMIS in this research can be downloaded from the official THEMIS website.

References

- Angelopoulos, V.: *Space Sci. Rev.* **141**, 5–34 (2008)
- Angelopoulos, V., et al.: *J. Geophys. Res.* **97**, 4027 (1992)
- Ashour-Abdalla, M., et al.: *Nat. Phys.* **7**, 360–365 (2011)
- Auster, H.U., et al.: *Space Sci. Rev.* **141**, 235–264 (2008)
- Birn, J., Nakamura, R., Panov, E.V., Hesse, M.: *J. Geophys. Res.* **116**, A01210 (2011)
- Birn, J., Runov, A., Hesse, M.: *J. Geophys. Res. Space Phys.* **119**, 3604–3616 (2014)
- Fu, H.S., et al.: *Geophys. Res. Lett.* **38**, L16104 (2011)
- Fu, H.S., et al.: *Geophys. Res. Lett.* **40**, 6023–6027 (2013)
- Guzdar, P.N., et al.: *Geophys. Res. Lett.* **37**, L20102 (2010)
- Huang, C., et al.: *J. Geophys. Res. Space Phys.* **120**, 1759–1765 (2015a)
- Huang, S.Y., et al.: *Astrophys. Space Sci.* **357**, 22 (2015b)
- Hwang, K.-J., et al.: *J. Geophys. Res.* **116**, A00I32 (2011)
- Lapenta, G., Bettarini, L.: *Geophys. Res. Lett.* **38**, L11102 (2011)
- Liu, J., et al.: *J. Geophys. Res. Space Phys.* **120**, 2516–2530 (2015)
- Lu, H.Y., et al.: *J. Geophys. Res. Space Phys.* **118**, 6019–6025 (2013)
- Lu, H.Y., et al.: *Geophys. Res. Lett.* **42**, 10,099–10,105 (2015a)
- Lu, S., et al.: *J. Geophys. Res. Space Phys.* **120**, 6286–6300 (2015b)
- Lu, S., Angelopoulos, V., Fu, H.: *J. Geophys. Res. Space Phys.* **121**, 9483–9500 (2016)
- McFadden, J.P., et al.: *Space Sci. Rev.* **141**, 277–302 (2008)
- Nakamura, M.S., Matsumoto, H., Fujimoto, M.: *Geophys. Res. Lett.* **29**(8), 1247 (2002a)
- Nakamura, R., et al.: *Geophys. Res. Lett.* **29**(20), 1942 (2002b)
- Nakamura, R., et al.: *J. Geophys. Res. Space Phys.* **118**, 2055–2072 (2013)
- Ohtani, S.I., Shay, M.A., Mukai, T.: *J. Geophys. Res.* **109**, A03210 (2004)
- Pan, Q., et al.: *J. Geophys. Res.* **117**, A12224 (2012)
- Panov, E.V., et al.: *Geophys. Res. Lett.* **37**, L08103 (2010)
- Pritchett, P.L.: *J. Geophys. Res. Space Phys.* **120**, 592–608 (2015)
- Pritchett, P.L., Coroniti, F.V.: *J. Geophys. Res.* **115**, A06301 (2010)
- Pritchett, P.L., Coroniti, F.V.: *Geophys. Res. Lett.* **38**, L10102 (2011)
- Runov, A., et al.: *Geophys. Res. Lett.* **36**, L14106 (2009)
- Runov, A., et al.: *J. Geophys. Res. Space Phys.* **118**, 744–755 (2013)
- Schmid, D., et al.: *Ann. Geophys.* **29**, 1537–1547 (2011)
- Sitnov, M.I., Swisdak, M., Divin, A.V.: *J. Geophys. Res.* **114**, A04202 (2009)
- Sitnov, M.I., et al.: *Geophys. Res. Lett.* **40**, 22–27 (2013)
- Vapirev, A.E., et al.: *J. Geophys. Res. Space Phys.* **118**, 1435–1449 (2013)
- Vogiatzis, I.I., et al.: *Ann. Geophys.* **33**, 63–74 (2015)
- Volwerk, M., et al.: *J. Geophys. Res.* **113**, A08S90 (2008)
- Walsh, A.P., et al.: *Ann. Geophys.* **27**, 725–743 (2009)
- Wang, H., et al.: *Astrophys. J.* **821**, 84 (2016)
- Wolf, R.A., et al.: *J. Geophys. Res.* **111**, A12218 (2006)
- Wu, M.Y., et al.: *J. Geophys. Res. Space Phys.* **118**, 4804–4810 (2013)
- Wu, M.Y., et al.: *J. Geophys. Res. Space Physics* **120**, 6320–6331 (2015)
- Xing, X., Wolf, R.A.: *J. Geophys. Res.* **112**, A12209 (2007)
- Zhou, M., et al.: *Geophys. Res. Lett.* **36**, L20107 (2009)
- Zhou, X.-Z., et al.: *J. Geophys. Res.* **115**, A00I03 (2010)